Nano Res. 2011, 4(11): 1136–1143
DOI 10.1007/s12274-011-0162-5
Research Article

ISSN 1998-0124
CN 11-5974/O4

Fabrication of Large Area High Density, Ultra-Low Reflection Silicon Nanowire Arrays for Efficient Solar Cell Applications

Subramani Thiyagu, B. Parvathy Devi, and Zingway Pei (✉)

Graduate Institute of Optoelectronic Engineering, Department of Electrical Engineering, Chung Hsing University, Taichung 40227, Taiwan, China

Received: 8 May 2011 / Revised: 5 July 2011 / Accepted: 7 July 2011

ABSTRACT

High density vertically aligned and high aspect ratio silicon nanowire (SiNW) arrays have been fabricated on a Si substrate using a template and a catalytic etching process. The template was formed from polystyrene (PS) nanospheres with diameter 30–50 nm and density 10^{10}/cm^2, produced by nanophase separation of PS-containing block-copolymers. The length of the SiNWs was controlled by varying the etching time with an etching rate of 12.5 nm/s. The SiNWs have a biomimetic structure with a high aspect ratio (~100), high density, and exhibit ultra-low reflectance. An ultra-low reflectance of approximately 0.1% was achieved for SiNWs longer than 750 nm. Well-aligned SiNW/poly(3,4-ethylenedioxy-thiophene):poly(styrenesulfonate) (PEDOT:PSS) heterojunction solar cells were fabricated. The n-type silicon nanowire surfaces adhered to PEDOT:PSS to form a core–sheath heterojunction structure through a simple and efficient solution process. The large surface area of the SiNWs ensured efficient collection of photogenerated carriers. Compared to planar cells without the nanowire structure, the SiNW/PEDOT:PSS heterojunction solar cell exhibited an increase in short-circuit current density from 2.35 mA/cm^2 to 21.1 mA/cm^2 and improvement in power conversion efficiency from 0.4% to 5.7%.

KEYWORDS

Ultra-low reflection, silicon nanowire, polystyrene nanosphere, heterojunction solar cell

1. Introduction

Silicon nanowires (SiNWs) have attracted much attention due to their potential applications in nanoscale electronic and optoelectronic devices [1–4], field-effect transistors [5], field emitters [6], chemical sensors [7], and solar cells [8, 9]. Various methods have been developed to prepare one-dimensional (1D) silicon nanostructures. These include laser ablation [10], physical vapor deposition [11], and chemical vapor deposition [12, 13] which all involve a bottom-up approach [14]. However, these methods often result in randomly oriented SiNWs, with diameters and lengths having a wide distribution, limiting their application in real optoelectronic devices. Nanoelectronics and nanooptoelectronics generally require vertically aligned, tunable length, single crystalline, and high-density nanowires to obtain processing compatibility.

For Si-based optoelectronic devices, such as photodetectors and solar cells, the high refractive index of silicon results in more than 40% of the incident light being reflected, which severely limits the performance of the optoelectronic devices [15]. A reduction in

Address correspondence to zingway.pei@gmail.com

optical reflectance can enhance the light harvesting of optoelectronic devices, especially solar cells, and increase their photocurrent [16–18]. In principle, vertically tapered sub-wavelength structures can suppress reflection over a wide spectral range due to the gradient refractive index of their biomimetic structure [19]. The spacing between the nanowires should be smaller than the wavelength of incident light in order to achieve optimal omni-directional antireflection [20]. In addition, the length of the nanowires should as long as possible to achieve broadband antireflection. This implies that the diameter of the nanowires should be small and the aspect ratio should be high in order to achieve ultra-low reflectance. A variety of techniques for fabricating antireflection nanostructures have been described [21–24]. These methods have not resulted in sub-wavelength structures with high density and high aspect ratio and the reflectance has not been sufficiently low for practical application. To achieve high aspect ratio, methods such as reactive ion etching (RIE) [25, 26] and electron cyclotron resonance (ECR) plasma etching [27, 28] have been employed. However, in these cases the high vacuum limits the possibility of volume production with low cost.

In recent years, a simple Ag catalytic etching technique has been used to prepare large-area, aligned SiNW arrays on single-crystal silicon wafers [29–32]. The location, size, length and orientation control of silicon nanowire arrays have been established by catalytic etching through a pre-patterned template. To avoid high cost photolithography, the templates were usually obtained by using self-assembly of polystyrene (PS) spheres with a diameter of around half a micrometer [33]. Further reducing the diameter and spacing of the PS spheres in the template could produce SiNWs with larger surface areas, which could enhance the photogenerated carrier collection efficiency in solar cells. In addition, small diameter SiNWs with higher aspect ratios could achieve ultra-low reflectance over a broad range of wavelengths. As a consequence, the production of silicon nanowires with sub-100 nm diameter and spacing is strongly motivated by the desire to achieve an ultra-low reflectance and excellent carrier collection efficiency along the radial direction. However, high surface-to-volume ratio in the silicon nanowires may limit the open-circuit voltage (V_{oc}) and fill factor (FF) of the resulting solar cells due to the increase in surface recombination [34]. The length of the nanowires should therefore be limited. In this work, we focus on the reflection and carrier collection of SiNWs. We demonstrate a convenient method for large-scale fabrication of silicon nanowire arrays with controlled length and orientation using a 30–50 nm closely packed PS nanosphere template with excellent antireflection properties. The reflectance of the silicon nanowires was measured using an ultraviolet–visible spectrometer over the spectral range 300–800 nm. To demonstrate the advantageous light-trapping and efficient carrier collection of the SiNWs, the hole conducting polymer poly(3,4-ethylenedioxy-thiophene): poly(styrenesulfonate) (PEDOT:PSS) was applied on the n-type SiNWs to form a heterojunction diode solar cell.

2. Experimental

2.1 Polystyrene (PS) nanosphere template formation

Figure 1 shows a schematic diagram of the fabrication of SiNW arrays using a polystyrene nanosphere template obtained by the modified block-copolymer nanopatterning method. In this experiment, (100) oriented n-type silicon substrates were used. The silicon substrates were cleaned with acetone in an ultrasonicator at room temperature for 10 min to remove any possible organic contamination. The silicon substrate was then heated in boiling Piranha solution (4:1 (*v*/*v*) H_2SO_4/H_2O_2). Following this, the silicon substrate was rinsed several times with deionized water. After cleaning, the PS nanospheres were fabricated by modified block-copolymer nanopatterning. The poly(styrene-b-methyl-methacrylate) (PS-b-PMMA) block-copolymer solution was prepared by dissolving PS-b-PMMA powder in toluene at a concentration of 10 mg/mL. The PS-b-PMMA solution was spin-coated on the Si substrate at 2,500 r/min for 100 s. The thickness of the PS-b-PMMA film was around 60 nm. The thin PS-b-PMMA film was then annealed at 180 °C in a vacuum oven for 24 h. This temperature is well above the glass transition temperature (T_g) of both PS and PMMA allowing nanophase separation. The PS-b-PMMA film was then immersed in heated

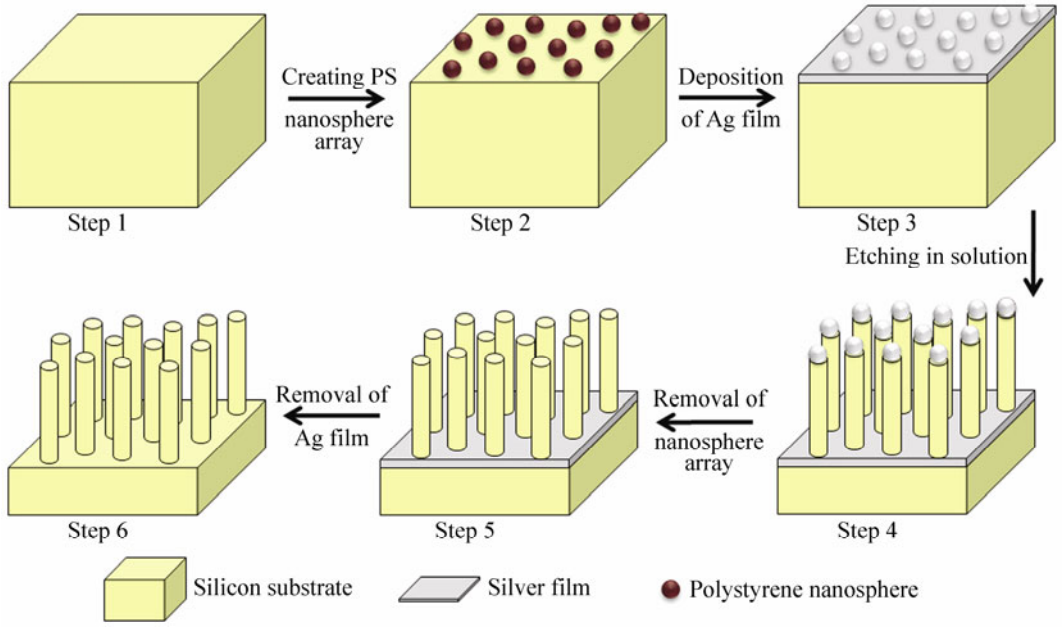

Figure 1 Schematic illustration of the fabrication of silicon nanowires using a template of polystyrene nanospheres based on modified block-copolymer nanopatterning

acetic acid and then rinsed in deionized water for 10 min to remove nanophase separated PMMA. PS nanospheres with a diameter of around 30–50 nm were subsequently obtained. This process was insensitive to the fabrication temperature and time. The density of the closely packed PS nanospheres, measured using scanning electron microscopy (SEM) (shown in Fig. 2), was as high as $10^{10}/cm^2$.

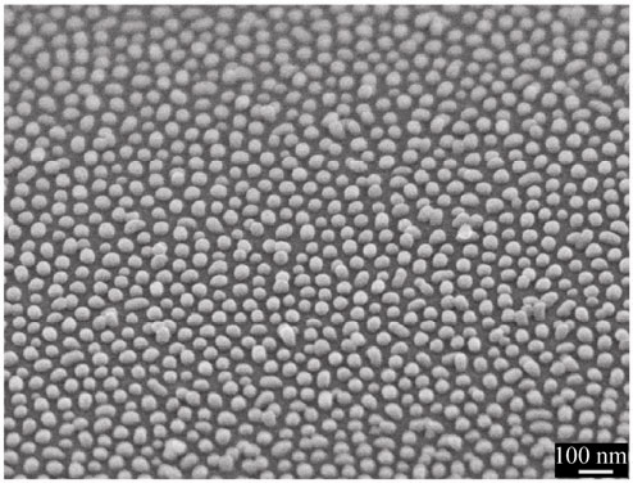

Figure 2 SEM image of the polystyrene nanospheres with diameter of 30 nm used as a template to form the nanowires

2.2 Fabrication of SiNWs

To accomplish silicon nanowire formation, chemical etching with a silver (Ag) catalyst was employed [33]. As in step 3 of Fig. 1, the silver film was deposited using a thermal evaporator at a rate of 1 Å/s. The thickness of the Ag films was 10 nm. A Teflon vessel was used as the container. For the solution etching process, an etching mixture consisting of HF, H_2O_2, and deionized water was used at room temperature. The concentrations of HF and H_2O_2 were 4.6 and 0.44 mol/L, respectively. The Ag layers adhering to the Si surfaces have a higher electronegativity than the Si, and electrons are therefore attracted to Ag from the Si, making the Aglayers negatively charged. The electrons from the negatively charged Ag layers are preferentially captured by the O^- ions of the H_2O_2 which become O^{2-} ions. This charge transfer causes local oxidation of the Si underneath the Ag patterns. The resulting SiO_2 was then continuously etched away by HF, leading to the penetration of Ag into the Si substrates.

The surfaces covered by the PS nanospheres do not possess this catalyzed chemical etching ability, resulting in Si nanowires with a diameter similar to the diameter of the PS nanospheres. The SiNWs were

obtained when the Ag penetration reached a certain depth. The etching duration was varied depending on the required length of the nanowires. After etching, the substrate was immersed in toluene for 1 h to remove the PS nanospheres. The silver film was then removed by immersing it in boiling aqua regia (3:1 (*v*/*v*) HCl/HNO_3) for 15 min.

2.3 Fabrication of SiNW/PEDOT:PSS heterojunction solar cells

To study the antireflection ability and carrier collection efficiency of the SiNWs, PEDOT:PSS was used to form a SiNW/PEDOT:PSS heterojunction solar cell [35]. The fabrication process involved the following steps. After removing the silver, the SiNWs were immersed in HF to remove the chemically contaminated oxide surface layer. Aluminum electrical contacts were deposited on the back of the SiNWs. Then, the PEDOT:PSS was spin-coated on the indium tin oxide (ITO)-coated glass rather than being directly spin-coated on the SiNW arrays. The top portion of the SiNWs was then immersed in the thin wet PEDOT:PSS film. The samples were subsequently annealed at 140 ˚C for 10 min in an effort to ensure that each individual SiNW became stuck to the PEDOT:PSS layer.

3. Results and discussion

Figure 3 shows images of the SiNW arrays fabricated on a n-type silicon substrate. Figure 3(a) shows a clear cross-sectional SEM image at a tilted angle (ca. 10°) of the SiNW arrays. The nanowires are seen to be distributed homogenously over a large area. Figures 3(b)–3(d) show high-magnification cross-sectional SEM images of SiNWs fabricated with different catalyst chemical etching times of 60, 90, and 240 s, producing nanowires with a length of around 700 nm, 1 μm, and 3 μm, respectively. The length of the silicon nanowires can be controlled and varies linearly with the duration of the catalyst etching process. The average etching rate for catalytic chemical etching for Si was 12.5 nm/s. Since the PS nanosphere template shown in Fig. 2 is aperiodic, the SiNWs are also randomly distributed with a high aspect ratio (from around 25 to 100). This structure is similar to that of antireflection feathers on the eyes of moths where the outer surface of the cornea is covered by an array of conical protuberances [27, 36]. The SiNWs should therefore have antireflection properties since the incident light undergoes multiple internal reflections causing a long optical path for absorption.

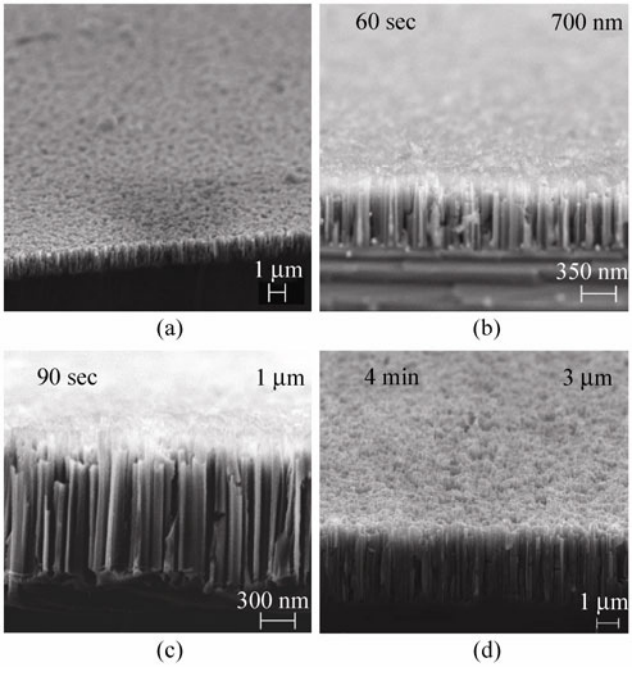

Figure 3 SEM image of silicon nanowire arrays: (a) cross-sectional image with tilted-view (ca. 10°) of silicon nanowire arrays distributed homogenously over a large area. High-magnification cross-sectional SEM images of samples after etching for (b) 60 s, (c) 90 s, and (d) 4 min

Indeed, only a small fraction of light was reflected back out, as has been reported in previous studies [37, 38]. Photographs of a polished bare Si wafer and a chemically etched substrate using an Ag catalyst are shown in the inset of Fig. 4. The prepared SiNW samples were black in appearance. The material can be named "black silicon" owing to the darkness of color. The reflectance spectra of the black SiNWs and the polished bare n-Si are shown in Fig. 4. The SiNWs show an ultra-low reflectance of approximately 0.1% over the entire spectral range from 300 to 800 nm. The ultra-low reflectance of SiNWs is caused by strong absorption due to the strong internal light trapping property of the dense SiNWs. This remarkable property suggests that these SiNW arrays are an appropriate candidate for antireflective surfaces and absorption materials used in photovoltaic cells.

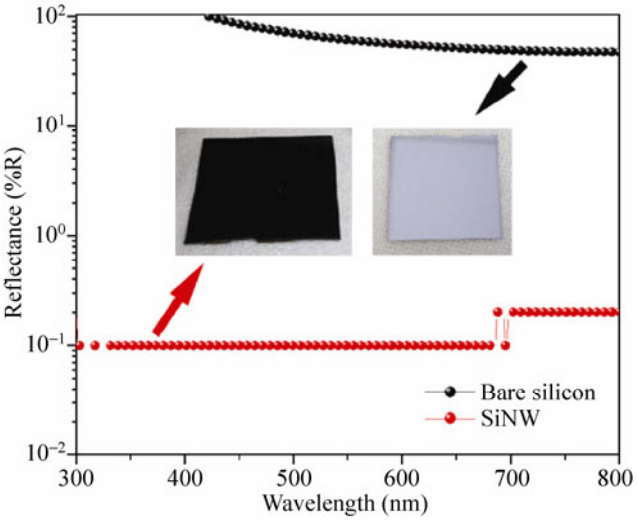

Figure 4 Reflectance as a function of wavelength for an n-SiNW array and a bare polished n-Si sample

The spectral reflectance of SiNWs fabricated using different etching times, ranging from 10 s to 180 s are shown in Fig. 5. Even an etching time of 10 s results in a drastic decrease in reflectance from over 40% for the polished Si wafer to less than 10% over the entire spectral range from 300 to 800 nm. The length of the Si nanowires after 10 s of chemical etching was around 125 nm, indicating why the closely packed SiNWs are a very efficient antireflection material. A further increase in etching time resulted in a more gradual decrease in reflectance. After 60 s, the reflectance approached 0.1%. The inset in Fig. 5 shows photographs of the three samples. One is bare silicon, and the other two are etched silicon (20 s and 2 min). The 20 s etched SiNWs appear light grey in color and the 120 sec etched SiNWs appear totally black.

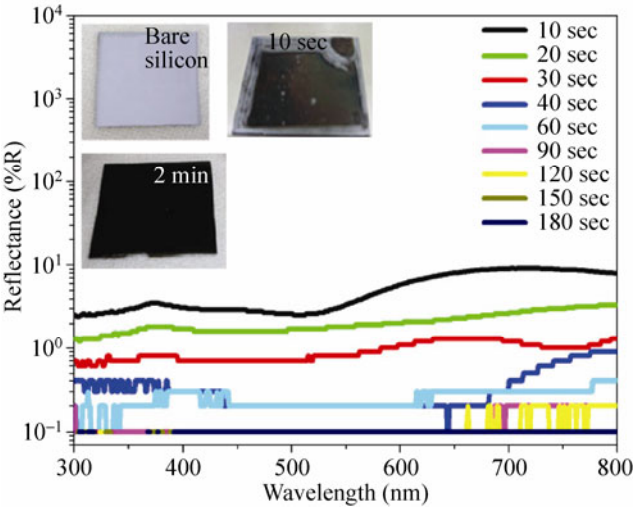

Figure 5 Reflectance spectra of SiNWs with different etching time from 10 s to 180 s

To demonstrate an application of the excellent antireflection property and study the efficiency of carrier collection by the SiNW arrays, a PEDOT:PSS conducting polymer was used as the p-type semiconductor on n-type SiNWs to form a heterojunction solar cell. The schematic structure of the SiNW/PEDOT:PSS photovoltaic cell is shown in Fig. 6(a).

The energy alignment of an ITO/PEDOT:PSS/n-SiNW/Al solar cell is sketched in Fig. 6(b). The highest occupied molecular orbital (HOMO) energy level for PEDOT:PSS is around 5.1 eV, which is similar to the valence band energy of Si.

The role of PEDOT:PSS is to build a Schottky contact to n-Si. With this contact, a barrier was built at the interface. After band alignment, an internal electrical field was established as schematically shown in Fig. 6(b). The photogenerated holes in SiNWs move toward PEDOT:PSS and the photogenerated electrons move along the SiNWs toward the Al contact to achieve the photovoltaic effect [35].

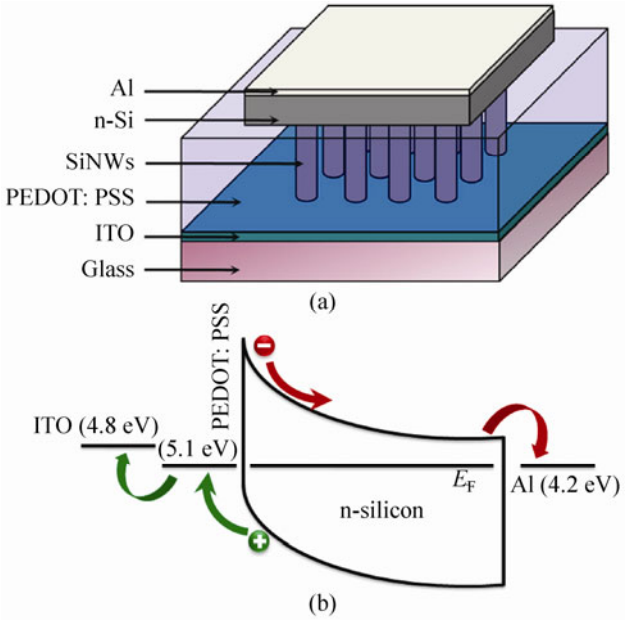

Figure 6 (a) Schematic diagram of the fabrication of a SiNW/PEDOT:PSS heterojunction solar cell. (b) Energy levels of the ITO/PEDOT:PSS/n-SiNW/Al solar cell

Figure 7 shows the dark current–voltage characteristics of the PEDOT:PSS on bare Si and SiNWs. The SiNW/PEDOT:PSS cell exhibits a higher forward current and lower reverse leakage current than the planar cell, implying the possibility of higher V_{oc} and FF, and lower series resistance. To validate this point, the photovoltaic effect of PEDOT:PSS on bare Si and on SiNWs was measured as depicted in Fig. 8. The *J*–*V* characteristics of the SiNW/PEDOT:PSS heterojunction solar cell were measured under an illumination intensity of 100 mW/cm² (AM 1.5G). For the PEDOT:PSS/bare Si heterojunction diode, the photocurrent density was relatively small. The values of short circuit current density (J_{sc}), V_{oc}, and FF were 2.35 mA/cm², 0.33 V, and 0.22, respectively, leading to a power conversion efficiency (PCE) of 0.4%. The details are listed in Table 1.

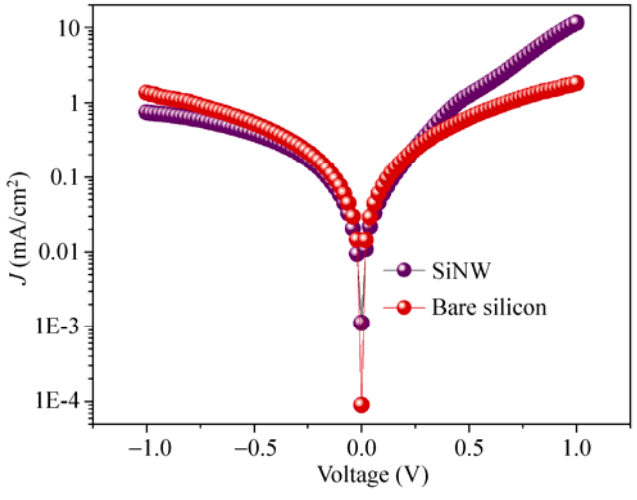

Figure 7 Dark current–voltage characteristics of the SiNW/PEDOT:PSS and planar Si/PEDOT:PSS solar cells

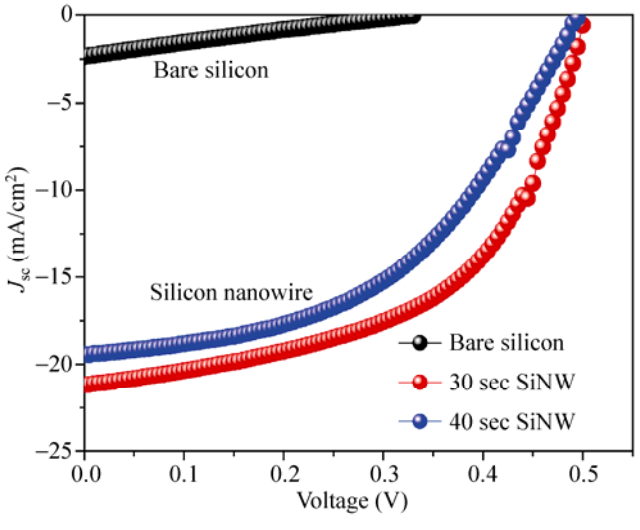

Figure 8 Photocurrent–voltage characteristics of the SiNW/PEDOT:PSS and planar Si/PEDOT:PSS solar cells

A marked increase in photovoltaic performance was observed in the case of the PEDOT:PSS/SiNWs heterojunction diode. The values of J_{sc}, V_{oc} and FF increased to 21.1 mA/cm², 0.50 V, and 0.53, respectively, leading to a PCE of 5.7%. Data for SiNWs chemically etched for different times and used in photovoltaic devices are listed in Table 1. The dramatic increase in photocurrent might result from the larger contact area and the shorter carrier diffusion distance. Possible reasons for the dramatic photocurrent enhancement are the efficient carrier collection and the antireflection properties. In the SiNW/PEDOT:PSS heterojunction solar cell, the large surface area of the SiNWs ensures a smaller contact resistance. In addition, the diffusion distance for photogenerated carriers is less than the diameter of SiNWs, which is around tens of nanometers. Therefore, the electron–hole pair separation and collection efficiency is greatly improved in the SiNW/PEDOT:PSS heterojunction solar cell as compared to the planar Si/PEDOT:PSS solar cell. To calculate the effective surface area for the SiNWs solar cell, values of the diameter, length, and density of 50 nm, 375 nm, and 10^{10}/cm² were used. On this basis, the effective area is 6.88 times more than the planar surface of the bare Si. However, the photocurrent of the SiNWs solar cell is almost 9 times higher than that of the planar Si solar cell. There is a 30% difference between calculation and experiment. Therefore, the antireflection ability of SiNWs might still be having an effect even though the light was illuminated onto the SiNWs through a glass substrate, ITO and PEDOT:PSS as shown in Fig. 6(a).

Table 1 Photovoltaic characteristics of the device

	J_{sc} (mA/cm²)	V_{oc} (V)	Fill factor	Efficiency (%)
Bare Si	2.35	0.33	0.22	0.4
30 s SiNWs	21.1	0.50	0.53	5.7
40 s SiNWs	19.4	0.49	0.47	4.61

4. Conclusions

We have fabricated large-area silicon nanowire arrays by catalytic etching through a 30–50 nm PS nanosphere template. The SiNWs exhibit a high density (10^{10}/cm^2), high aspect ratio (~100) and give an ultra-low reflectance of approximately 0.1% for wavelengths ranging from 300 to 800 nm, which is a suitable reflectance for use in solar cells. SiNW/PEDOT:PSS heterojunction photovoltaic devices were also fabricated. A high short-circuit current density of 21.1 mA/cm^2 was measured in SiNW/PEDOT:PSS heterojunction photovoltaic devices corresponding to a PCE of 5.7%. The high short-circuit current density suggests the as-fabricated SiNWs may possibly be employed in high efficiency solar cells.

Acknowledgements

We thank the National Science Council for financial support under grant No. NSC-99-ET-E-005-001-ET.

References

[1] Cui, Y.; Lieber, C. M. Functional nanoscale electronic devices assembled using silicon nanowire building blocks. *Science* **2001**, *291*, 851–853.

[2] Wang, D.; Sheriff, B. A.; McAlpine, M.; Heath, J. R. Development of ultra-high density silicon nanowire arrays for electronics applications. *Nano Res.* **2008**, *1,* 9–21.

[3] Ma, D. D. D.; Lee, C. S.; Au, F. C. K.; Tong, S. Y.; Lee, S. T. Small-diameter silicon nanowire surfaces. *Scienc.* **2003**, *299*, 1874–1877.

[4] Li, D. Y.; Wu, Y. Y.; Kim, P.; Shi, L.; Yang, P. D. Thermal conductivity of individual silicon nanowires. *Appl. Phys. Lett.* **2003**, *83*, 2934–2936.

[5] Goldberger, J.; Hochbaum, A. I.; Fan, R.; Yang, P. D. Silicon vertically integrated nanowire field effect transistors. *Nano Lett*. **2006**, *6*, 973–977.

[6] Wang, Q.; Li, J. J.; Ma, Y. J.; Bai, X. D.; Wang, Z. L.; Xu, P.; Shi, C. Y.; Quan, B. G.; Yue, S. L.; Gu, C. Z. Field emission properties of carbon coated Si nanocone arrays on porous silicon. *Nanotechnology* **2005**, *16*, 2919–2922.

[7] Shao, M. W.; Yao, H.; Zhang, M. L.; Wong, N. B.; Shan, Y. Y.; Lee, S. T. Fabrication and application of long strands of silicon nanowires as sensors for bovine albumin detection. *Appl. Phys. Lett.* **2005**, *87*, 183106.

[8] Zhu, J.; Hsu, C. M.; Yu, Z.; Fan, S.; Cui, Y. Nanodome solar cells with efficient light management and self-cleaning. *Nano Lett*. **2010**, *10*, 1979–1984.

[9] Fan, Z.; Ruebusch, D. J.; Rathore, A. A.; Kapadia, R.; Ergen, O.; Leu, P. W.; Javey, A. Challenges and prospects of nanopillar-based solar cells. *Nano Res.* **2009**, *2*, 829–843.

[10] Morales, A. M.; Lieber, C. M. A laser ablation method for the synthesis of crystalline semiconductor nanowires. *Science* **1998**, *279*, 208–211.

[11] Yu, D. P.; Bai, Z. G.; Ding, Y.; Hang, Q. L.; Zhang, H. Z.; Wang, J. J.; Zou, Y. H.; Qian, W.; Xiong, G. C.; Zhou, H. T.; Feng, S. Q. Nanoscale silicon wires synthesized using simple physical evaporation. *Appl. Phys. Lett.* **1998**, *72*, 3458–3460.

[12] Kim, B. S.; Koo, T. W.; Lee, J. H.; Kim, D. S.; Jung, Y. C.; Hwang, S. W.; Choi, B. L.; Lee, E. K.; Kim, J. M.; Whang, D. Catalyst-free growth of single-crystal silicon and germanium nanowires. *Nano Lett.* **2009**, *9*, 864–869.

[13] Liu, X.; Wang, D. Kinetically-induced hexagonality in chemically grown silicon nanowires. *Nano Res.* **2009**, *2*, 575–582.

[14] Whang, D.; Jin, S.; Wu, Y.; Lieber, C. M. Large-scale hierarchical organization of nanowire arrays for integrated nanosystems. *Nano Lett.* **2003**, *3*, 1255–1259.

[15] Doshi, P.; Jellison, G. E.; Rohatgi, A. Characterization and optimization of absorbing plasma-enhanced chemical vapor deposited antireflection coatings for silicon photovoltaics. *Appl. Opt*. **1997**, *36*, 7826–7837.

[16] Striemer, C. C.; Fauchet, P. M. Dynamic etching of silicon for broadband antireflection applications. *Appl. Phys. Lett*. **2002**, *81*, 2980–2982.

[17] Lee, Y. J.; Ruby, D. S.; Peters, D. W.; McKenzie, B. B.; Hsu, J. W. P. ZnO nanostructures as efficient antireflection layers in solar cells. *Nano Lett*. **2008**, *8*, 1501–1505.

[18] Gombert, A.; Glaubitt, W.; Rose, K.; Dreibholz, J.; Blasi, B.; Heinzel, A.; Sporn, D.; Doll, W.; Wittwer, V. Antireflective transparent covers for solar devices. *Sol. Energy.* **2000**, *68*, 357–360.

[19] Li, Y.; Zhang, J.; Yang, B. Antireflective surface based on biomimetic nanopillared arrays. *Nano Today* **2010**, *5*, 117–127.

[20] Wilson, S. J.; Hutley, M. C. The optical properties of moth eye antireflection surfaces. *Opt. Acta* **1982**, *29*, 993–1009.

[21] Heine, C.; Morf, R. H. Submicrometer gratings for solar energy applications. *Appl. Opt.* **1995**, *34*, 2476–2482.

[22] Kanamori, Y.; Roy, E.; Chen, Y. Antireflection subwavelength gratings fabricated by spin-coating replication. *Microelectron. Eng.* **2005**, *78–79*, 287–293.

[23] Aydin, C.; Zaslavsky, A.; Sonek, G. J.; Goldstein, J. Reduction of reflection losses in $ZnGeP_2$ using motheye antireflection surface relief structures. *Appl. Phys. Lett.* **2002**, *80*, 2242–2244.

[24] Zhang, G. M.; Zhang, J.; Xie, G. Y.; Liu, Z. F.; Shao, H. B. Cicada wings: A stamp from nature for nanoimprint lithography. *Small* **2006**, *2*, 1440–1443.

[25] Min, W. L.; Jiang, B.; Jiang, P. Bioinspired self-cleaning antireflection coatings. *Adv. Mater.* **2008**, *20*, 3914–3918.

[26] Wang, Y; Lu, N.; Xu, H.; Shi, G.; Xu, M.; Lin, X.; Li, H.; Wang, W.; Qi, D.; Lu, Y.; Chi, L. Biomimetic corrugated silicon nanocone arrays for self-cleaning antireflection coatings. *Nano Res*. **2010**, *3*, 520–527.

[27] Huang, Y. F.; Chattopadhyay, S.; Jen, Y. J.; Peng, C. Y.; Liu, T. A.; Hsu, Y. K.; Pan, C. L.; Lo, H. C.; Hsu, C. H.; Chang, Y. H.; Lee, C. S.; Chen, K. H.; Chen, L. C. Improved broadband and quasi-omnidirectional anti-reflection properties with biomimetic silicon nanostructures. *Nat. Nanotechnol.* **2007**, *2*, 770–774.

[28] Ting, C. J.; Huang, M. C.; Tsai, H. Y.; Chou, C. P.; Fu, C. C. Low cost fabrication of the large-area anti-reflection films from polymer by nanoimprint/hot-embossing technology. *Nanotechnology* **2008**, *19*, 205301.

[29] Peng, K. Q.; Yan, Y. J.; Gao, S. P.; Zhu, J. Synthesis of large area nanowire via self-assembling nanoelectrochemistry. *Adv. Mater.* **2002**, *14*, 1164–1167.

[30] Peng, K. Q.; Huang, Z. P.; Zhu, J. Fabrication of large-area silicon nanowire p–n junction diode arrays. *Adv. Mater.* **2004**, *16*, 73–76.

[31] Peng, K. Q.; Wu, Y.; Fang, H.; Zhong, X. Y.; Xu, Y.; Zhu, J. Uniform, axial-orientation alignment of one-dimensional single-crystal silicon nanostructure arrays. *Angew. Chem. Int. Edn.* **2005**, *44*, 2737–2742.

[32] Peng, K. Q.; Hu, J. J.; Yan, Y. J.; Wu, Y.; Fang, H.; Xu, Y.; Lee, S. T.; Zhu, J. Fabrication of single-crystalline silicon nanowires by scratching a silicon surface with catalytic metal particles. *Adv. Funct. Mater.* **2006,** *16*, 387–394.

[33] Huang, Z.; Fang, H.; Zhu, J. Fabrication of silicon nanowire arrays with controlled diameter, length, and density. *Adv. Mater.* **2007**, *19*, 744–748.

[34] Garnett, E.; Yang, P. Light trapping in silicon nanowire solar cells. *Nano Lett*. **2010**, *10*, 1082–1087.

[35] Shiu, S. C.; Chao, J. J.; Hung, S. C.; Yeh, C. L.; Lin, C. F. Morphology dependence of silicon nanowire/poly(3,4-ethylenedioxythiophene):poly(styrenesulfonate) heterojunction solar cells. *Chem. Mater*. **2010**, *22*, 3108–3113.

[36] Clapham, P. B.; Hutley, M. C. Reduction of lens reflection by moth eye principle. *Nature* **1973**, *244*, 281–282.

[37] Tsakalakos, L. Nanostructures for photovoltaics. *Mater. Sci. Eng. R.* **2008**, *62*, 175–189.

[38] Muskens, O. L.; Rivas, J. G.; Algra, R. E.; Bakkers, E. P. A. M.; Lagendijk, A. Design of light scattering in nanowire materials for photovoltaic applications. *Nano Lett*. **2008**, *8*, 2638–2642.